DEVELOPMENT OF THE SPACE DEBRIS SENSOR

J. Hamilton[(1)], J.-C. Liou[(1)], P.D. Anz-Meador[(2)], B. Corsaro[(3)], F. Giovane[(3)], M. Matney[(1)], E. Christiansen[(1)]

[(1)] NASA Johnson Space Center, Houston, TX 77058, [(2)]Jacobs, NASA Johnson Space Center, Houston, TX 77058, [(3)]LZT-Jacobs JETS Contract, NASA Johnson Space Center, Houston, TX 77058

ABSTRACT

The Space Debris Sensor (SDS) is a NASA experiment scheduled to fly aboard the International Space Station (ISS) starting in 2017. The SDS is the first flight demonstration of the Debris Resistive/Acoustic Grid Orbital NASA-Navy Sensor (DRAGONS) developed and matured by the NASA Orbital Debris Program Office. The DRAGONS concept combines several technologies to characterize the size, speed, direction, and density of small impacting objects. With a minimum two-year operational lifetime, SDS is anticipated to collect statistically significant information on orbital debris ranging from 50 μm to 500 μm in size.

This paper describes the SDS features and how data from the ISS mission may be used to update debris environment models. Results of hypervelocity impact testing during the development of SDS and the potential for improvement on future sensors at higher altitudes will be reviewed.

1 INTRODUCTION

To estimate the number and sizes of small debris objects in low Earth orbit (LEO), the region below 2000 km altitude), scientists have inspected hardware that has been exposed to the LEO environment under known conditions and then returned to earth. Since the Space Shuttle stopped flying in 2011, very little hardware has returned from space in a condition suitable for counting orbital debris impacts.

Orbital debris about 10 cm or larger in LEO, and about 1 m or larger in the geosynchronous orbit region are tracked by the U.S. Space Surveillance Network and maintained in the U.S. Satellite Catalog. The NASA Orbital Debris Program Office (ODPO) maintains an on-going program that uses the Haystack Ultrawideband Satellite Imaging Radar, the Haystack Auxiliary Radar, and Goldstone radars to collect data for orbital debris as small as several millimeters in LEO. For orbital debris smaller than 1 millimeter in LEO, space-based *in-situ* measurements and the inspection of external hardware surfaces returned from space are the only options. The most recent data on the sub-millimeter orbital debris population came from the inspection of the Hubble Space Telescope Wide Field Planetary Camera 2 radiator surface (exposed to space between 1993 and 2009) and the window and radiator panels of the Orbiter from Space Shuttle missions between 1995 and 2011. Since the orbits of sub-millimeter orbital debris evolve rapidly in the LEO environment, updated data are needed on a regular basis to better define the population and to quantify the risk to operational spacecraft. An alternative to inspecting returned hardware was needed to continue measuring this dynamic environment.

A key difficulty for *in-situ* measurements of small micrometeoroid and orbital debris (MMOD) is achieving a large enough detection area and long enough exposure time to collect sufficient data for meaningful statistical sampling of the population. For a 3-year mission at the high LEO altitudes (700-1000 km altitude), a detection area of 1 m^2 in the optimal pointing direction is the minimum requirement.

Several *in-situ* methods were considered to characterize debris objects too small to be measured by ground radars. A promising solution, the Space Debris Sensor (SDS), has been developed and is ready to fly as a NASA experiment scheduled aboard the International Space Station (ISS) starting in 2017. For a planned 2-year mission at the ISS altitude of about 400 km altitude, a detection area of 1 m^2 is sufficient to demonstrate the technology and to sample the orbital debris population less than 500 μm in size. The SDS is the first flight demonstration of the Debris Resistive/Acoustic Grid Orbital NASA-Navy Sensor (DRAGONS) developed and matured by the NASA ODPO. To avoid unnecessary confusion with SpaceX's Dragon spacecraft, which will carry the sensor to the ISS, the operational name used for the ISS DRAGONS mission is SDS.

2 THE DRAGONS CONCEPT

The NASA ODPO has supported development of particle impact detection technologies since 2002 [1, 2]. The ultimate goal is to conduct *in-situ* measurements to better characterize the small MMOD populations in the near-Earth environment, especially in LEO where many critical NASA spacecraft, including the ISS, the Hubble Space Telescope, and the Earth Observing System, operate. Due to the high impact speed in LEO (with an average of 10 km/sec, but as high as 14 km/sec for satellites in sun-synchronous orbits), orbital debris as small as 0.3 mm are a safety concern for human space

flight and robotic missions. Similar risks also come from small micrometeoroids (but with higher impact speeds).

The ODPO has supported development of DRAGONS, a combined technology impact sensor, to address the lack of new data for orbital debris in the millimeter and smaller size regime. Early DRAGONS technology development was also funded, via two multi-year proposal awards, by the NASA Science Mission Directorate and the NASA Exploration System Mission Directorate. The DRAGONS team consists of members from several organizations, including the NASA ODPO, the U.S. Naval Academy, the U.S. Naval Research Laboratory, the University of Kent in Great Britain, Virginia Tech, the Johnson Space Center (JSC) Hypervelocity Impact Technology (HVIT) group, and the Jacobs JSC Engineering, Technology and Science contract team. NASA ODPO proposed DRAGONS as an external payload on the ISS to the ISS Technology Demonstration Office in 2014. The proposal was accepted, including the payload funding support, by the ISS Program in early 2015. The plan is to deploy a 1 m^2 DRAGONS on the ISS in late 2017 for a 2- to 3-year mission duration.

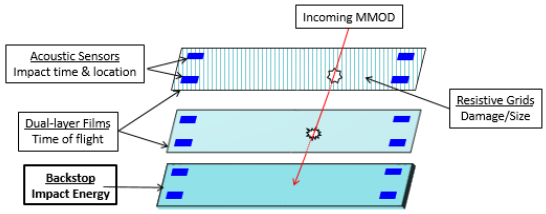

Figure 1. The three-layer DRAGONS structure

The basic structure of a DRAGONS unit is illustrated in Fig. 1. It includes two thin films located 15 cm apart. A solid backstop plate also is placed at a short distance below the second thin film. Multiple acoustic impact sensors are attached to the thin films and the back plate. The surface of the two films is coated with long and 75-µm wide resistive lines. When a hypervelocity MMOD particle, sufficiently larger than the thickness of the two thin films and the width of the resistive lines, hits the first film, it will cut one or more resistive lines, travel through the film, impact the second film, go through it, and then finally hit the backstop plate. The impact location on the top (or the bottom) film can be calculated with a simple triangulation algorithm based on the different signal arrival times measured by different acoustic sensors [3]. Combining the impact timing and location data on the two films provides the impact speed and direction measurements of the impacting particle. Hypervelocity impact experiments have shown that, for thin film penetration, the damage area is approximately 5-10% larger than the size of the impacting particle. A more accurate correlation can be established by dedicated hypervelocity impact tests. Therefore, the resistance increase of the grid panel at the time of the impact (signalled by the acoustic sensors) indicates the number of line breaks, which is a good measure of the size of the damage area. When the particle finally hits the solid back plate, the impact kinetic energy can be estimated from the acoustic signals received by the sensors attached to the plate. When data from these measurements are processed and combined, information on the impact time, location, speed, direction, size of the impacting particle, and a simple estimate of the material density of the impacting particle can be obtained. An example of a hypervelocity impact test on a DRAGONS prototype unit is shown in Fig. 2.

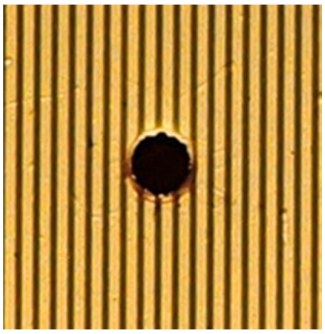

Figure 2. Example of damage to first sensor layer from a 0.4 mm diameter stainless steel spherical projectile at 7 km/s and 30° impact angle (it broke three lines)

3 THE SDS ON ISS

With a minimum 2-year operational lifetime, SDS is anticipated to collect statistically significant information on orbital debris ranging from 50 µm to 500 µm in size. Below 50 µm, the impact energy may be too small to detect or characterize. Above 500 µm, impacts are possible and will be measured, but are less likely according to our current model of the environment.

SDS is constructed with two resistive grid layers approximately 15 cm apart, with a Lexan backstop 5 cm behind the second grid layer. Each layer, approximately 1 m^2 in area, is equipped with acoustic sensors, acoustic calibration sources, and temperature measurement devices, shown in Fig. 3. Acoustic sensors are indicated in blue, acoustic calibration sources in red.

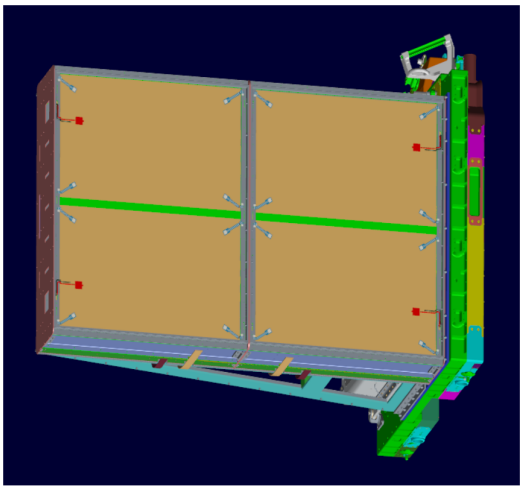

Figure 3. An isometric view of the SDS as ready for installation aboard the ISS and shown integrated with the Columbus External Payload Adapter, but without thermal blankets

The SDS will be hosted aboard ISS on the *Columbus* module External Payload Facility (EPF)-Starboard Overhead X-location (SOX), as indicated in Fig. 4.

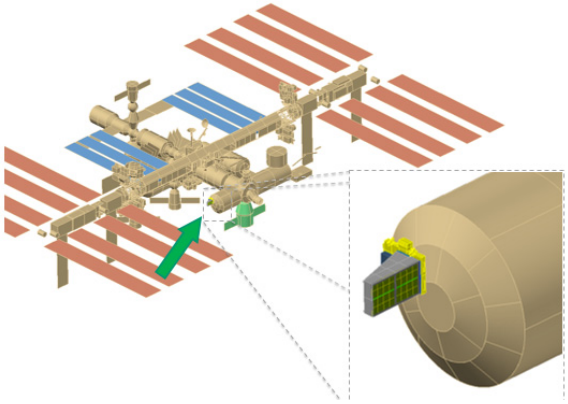

Figure 4. The ESA Columbus module's External EPF-SOX location.

This location was previously used by the European Technology Exposure Facility (EuTEF); among the EuTEF payloads were two Debris In Orbit Evaluator standard MMOD measurement sensors exposed for approximately 1.57 years (15 February 2008 – 1 September 2009), which may enable a future, decadal comparison. The robotic SDS installation will mount SDS's surface normal within 5° of the ISS ram direction. The torque-equivalent attitude flown by the ISS, as well as other excursions from nominal flight attitude will alter this orientation; however, ISS attitude is recorded for data reduction and analysis so these effects are mitigated.

In addition to health and status data, including time and ISS position and attitude, a 1 Hz data stream records grid resistance and temperature; a 500 kHz data stream records the acoustic excitation of a surface once an impact is detected. SDS first layer field of view (FOV) is approximately 2π sr. However, the effective first-layer FOV is diminished by permanent or transient occultation, as portrayed in Fig. 5.

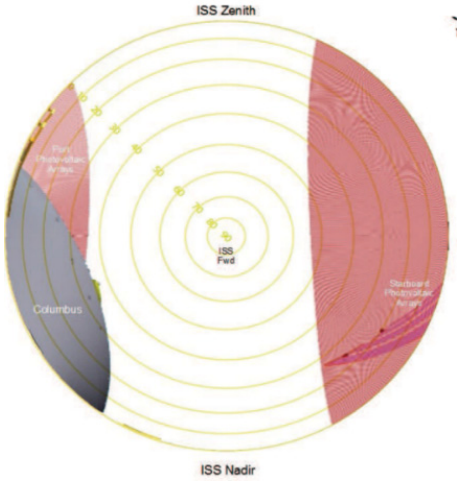

Figure 5. Columus EPF-SOX ram-direction field of view.

Visible is the *Columbus* module body at lower left and partial obscuration by the ISS port and starboard photovoltaic arrays. Note that these arrays will sweep through the FOV at various orientations and are not indicative of complete obscuration. The hemispherical map is easily converted to a local azimuth-elevation-obscuration flux mask. The mask is used with SDS performance simulator software when estimating the number of impacts expected in the Orbital Debris Engineering Model (ORDEM) 3.0 and Meteoroid Environment Model (MEM) Release 2 environments.

SDS three-layer FOV is decreased by the depth of sensor, yielding an SDS acceptance solid angle $< 2\pi$ sr. Simulations and hypervelocity impact (HVI) testing indicates that a portion of the first-layer impacts will fail to impact the backstop because their trajectory lies outside the acceptance angle or because they fragment upon impact with the first or second layer.

4 DEVELOPMENTAL TESTING

Nearly 100 hypervelocity impact tests were performed to (1) select the SDS configuration, (2) obtain data to characterize the response of the SDS to hypervelocity impacts as a function of projectile size, density, and impact velocity and angle, and (3) verify the response of

the flight hardware including the data acquisition system. The tests were planned and coordinated by the JSC HVIT group and performed at the NASA White Sands Test Facility (WSTF). WSTF hypervelocity launchers are shown in Fig. 6, while Table 1 provides a synopsis of the hypervelocity impact tests. Fig. 2 provides an example of the damage to the first sensor layer from one of the impact tests.

In addition to hypervelocity impact testing conducted at NASA WSTF, some proof-of-concept testing was conducted at NASA JSC's Experimental Impact Laboratory (EIL) using their Light Gas Gun and Vertical Gun. These campaigns are summarized in Table 2.

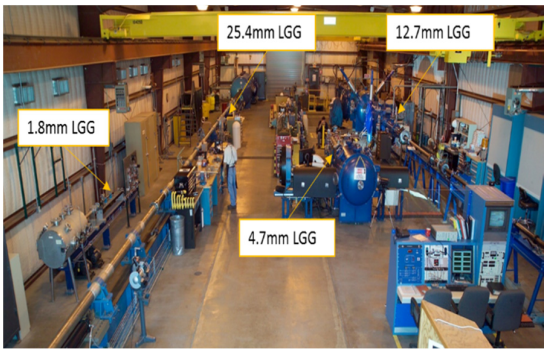

Figure 6. WSTF two-stage light gas gun launchers with second stage bore diameter indicated

Table 1. Summary of WSTF Hypervelocity Impact Tests on SDS

Test Series	Number of Tests	Projectile Material Types	Projectile Diameter* Range (mm)	Projectile Velocity Range (km/s)	Projectile Impact Angle* Range (deg)	Test Objectives
Initial	10	Al 2017-T4, stainless steel	0.3 – 1.0	6.95 – 7.23	0 - 45	Evaluate sensor configuration options.
1	9	Al 2017-T4, stainless steel, plastic	0.50	7.04 – 7.32	45	Obtain data to characterize response to range of projectile densities.
2	14	Al 2017-T4, stainless steel, aluminum oxide, plastic	0.20 – 0.50	5.01 – 8.40	0 - 60	Characterize response of sensor systems to changes in projectile size, velocity and density.
3	7	Al 2017-T4 and stainless steel	0.40 – 0.50	6.81 – 7.24	0	Investigate anomalous resistance changes in resistive grid and evaluate methods to prevent the issue.
4	9	Stainless steel	0.50	6.68 – 7.21	0 - 45	Confirm resistance change with number of line breaks and obtain velocity data.
5	6	Al 2017-T4, stainless steel, aluminum-oxide	0.2 – 0.40	6.90 – 7.25	0	Obtain acoustic and resistance data from sensor layers. Evaluate prototype data acquisition system.
6	43	Al 2017-T4, stainless steel, aluminum-oxide	0.2 - 1.0	4.70 - 7.64	0 - 72	High-fidelity test article (flight-like): Demonstrate ability to detect impactor size, speed and density. Demonstrate flight data acquisition system/software.

Notes:
Projectiles are spheres. Density of Al 2017-T4 is 2.796 g/cm^3, Stainless steel density is 7.667 g/cm^3, aluminum oxide density is 3.9 g/cm^3, plastic density is 1.14 g/cm^3.
Impact angle measured from target normal; i.e., 0 deg impact is normal to the target.

Table 2. Summary of EIL developmental SDS testing

Test Series	Number of Tests	Projectile Material Types	Projectile Diameter* Range (mm)	Projectile Velocity Range (km/s)	Projectile Impact Angle* Range (deg)	Test Objectives
E1	13 + 2*	Al 2024, soda lime glass (SLG)	0.20-1.00	5.57 – 5.96	25-39	evaluate methods to prevent anomalous resistance changes and choose solution
E2	4	Al 2017-T4	0.30 – 0.40	4.65 – 5.02	30	Characterize response of sensor systems using flight hardware and software

Notes:

*conducted on EIL Vertical Gun. Projectiles are spheres. Density of Al 2017-T4 is 2.796 g/cm^3, Al 2024 is 2.768 g/cm^3, and soda lime glass (SLG) is 2.45 g/cm^3. Impact angle measured from target normal; i.e., 0 deg impact is normal to the target.

4.1 Impact Location Determination/Accuracy

One key to calculating particle direction and speed is an accurate determination of the impact location. For the Dragons system we identify this location using acoustic sensors. The particle impact on each layer generates vibrational waves traveling on the film. The arrival time of these waves can be measured using strain sensors placed at various locations on the surface. Comparing these various signal arrival times from sensors placed at different locations, a geometrical algorithm identifies the impact location.

This type of geometrical calculation, using only signal arrival times at known locations, is called multilateration. While the calculation can be quite involved, we determined that the procedure could be reduced to a simple set of algebraic equations for any group of three orthogonally located sensors. The Dragons sensor installation makes use of this significant simplification by locating sensors in a rectangular array, with four sensors in each film section. While only three sensors are needed, the inclusion of a fourth improves the accuracy of the measurement and provides a backup should one sensor fail.

For this application on thin, low-modulus films, it is important that the strain sensor does not significantly constrain the motion of the wave. The thin, flexible sensor material selected is poly-vinylidene fluoride. It is a piezoelectric; when strained it produces an electrical signal (charge) that is proportional to the strain.

The sensor locations, the wave speed on the material (monitored using the on-board pinger as a reference source), and the signal arrival times at each sensor location are used to determine the impact location. While the last of these might appear simple, several issues can degrade arrival time accuracy. The arriving strain wave is not a sudden sharp transition, but rather is more gradual with some complexity. In part this is because as the wave travels from the point of impact to the sensor location, it is dispersive – that is, it has a broad frequency spectrum with both attenuation and speed being strong functions of frequency. Additionally, various types of waves are generated by the impact (shear, longitudinal, surface, etc.), each traveling simultaneously with different speeds, and exchanging energy (mode conversion). Various complicated algorithms are available for sharpening the signal wave front, but for present purposes, a simpler procedure is used: limiting the bandwidth to frequencies above 30 kHz to reduce low frequency modal excitations, and identifing the (relative) signal arrival time as the time where some fraction (typically 15%) of the signal energy has arrived.

Laboratory versions of this combined sensor system were built and evaluated. The final test article was fabricated to be identical to the top half-section of the SDS array. Comparing true and calculated impact locations found the procedure has an average deviation of 0.8 cm. All measured values were within or very near the 3 cm measurement error required for this unit as shown in Fig. 7 and Fig. 8. While this accuracy is sufficient for now, it is expected to be reduced in the future as additional calibration tests are performed.

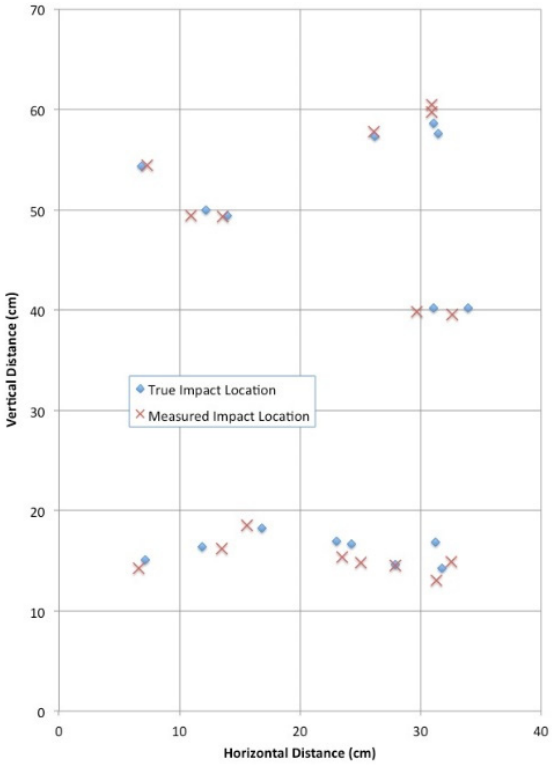

Figure 7. Impact Location Accuracy Test Results

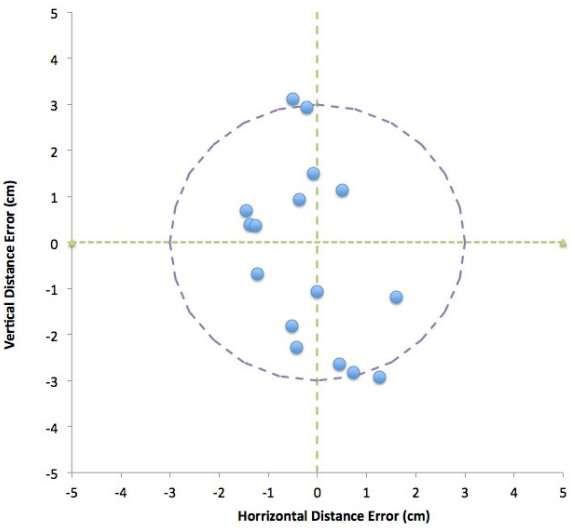

Figure 8. Impact Location Measurement Errors

4.2 Trajectory & Velocity/Accuracy

Having determined the impact locations on the two films and their (known) separation distance, it is a simple matter to calculate the particle's direction of impact. While the measured trajectory is actually over the path between the films, it is reasonable to assume that the particle direction of travel was not changed significantly by its impact with the first thin film layer. This is verified by the following data.

For most of the data, the incident angles were set at 30 or 60 degrees from perpendicular in the Y-axis direction. Using the impact locations determined from the acoustic signals, the errors in the determined X- and Y-axis directions are shown in the Fig. 9. The average deviation is 3.0° with all but two tests producing values within 10° of true.

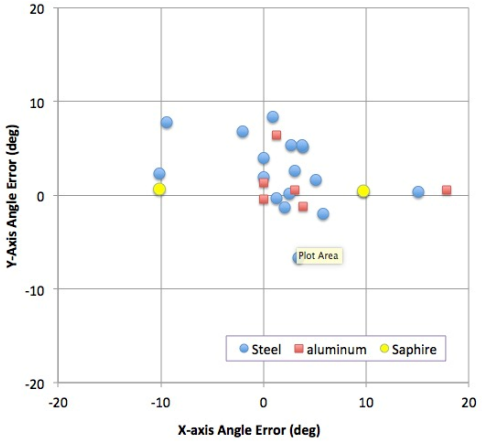

Figure 9. Angular Measurement Errors

To calculate the object's speed, the distance the particle travels between the two layers must be measured. This is found using the known layer separation distance and the above direction of travel. The impact time on each layer is identified via the same multilateral calculation that identifies location. Then this time difference and the travel distance can directly give the particle speed in the space between the two layers, assuming the particle is not significantly slowed by its impact with the first film. The resulting calculated particle speeds are graphed against the true speed in Fig. 10. The average difference is 18%.

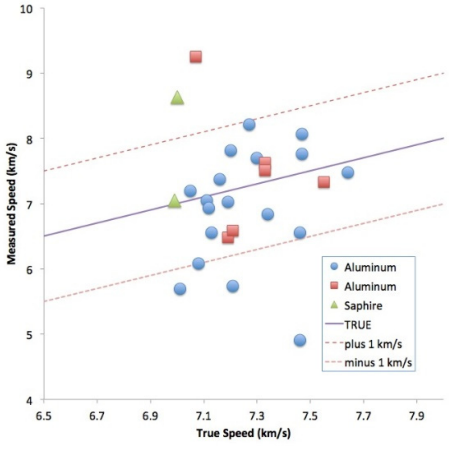

Figure 10. Sensor Measured Speed vs. true Speed

The uncertainties in these parameters principally are related to the uncertainty in measuring the signal arrival times. At present the average error in determining the signal arrival time is ±4.5 micro-seconds. While this is acceptable for present purposes, improvements are anticipated as more calibration data is obtained.

4.3 Penetrator Density/Accuracy

The acoustic amplitudes also provide a way of distinguishing particle material. Debris can be classified as high, medium, or low density, represented by the materials stainless steel, aluminum, and plastic. All materials of interest can be assigned in one of these three groups depending on its density and fragility; for example, glass would be classified in the low-density group. The impact characteristics of particles in these three groups are different and can be distinguished using the acoustic signal information.

Plastic and glass particles are easily distinguished from the metal particles. For these materials the signals on the second layer are always smaller than signals on the first layer, largely due to lack of penetration or particle fracture or disintegration.

Steel and aluminum particles (in the size range of interest) easily penetrate the first layer. They typically produce larger signals on the second layer than on the first, as they are accompanied by the additional mass (spray) of material removed from the first layer.

For particles that penetrate both film layers and impact the backing plate, the energy contained in the acoustic signals will be related to the (remaining) kinetic energy of the particle. Since the speed is known, this provides a value for its mass, and having determined its size, can obtain a measure of its density. Since the small errors in speed and diameter (cubed) will accumulate, this is only approximate; however, as shown in Fig. 11, this is sufficient to clearly distinguish steel from aluminum particles of the same size.

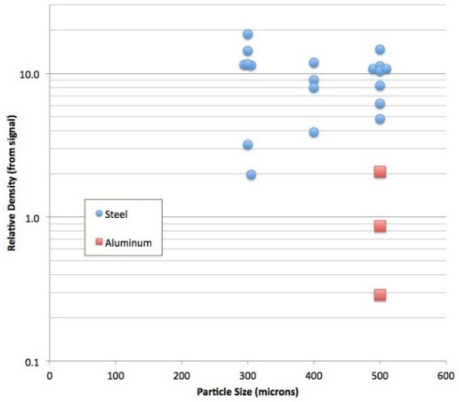

Figure 11. Measuring the Density of Debris

Aluminum particles smaller than 0.4 mm typically do not reach the backstop layer with sufficient energy to generate a detectable signal. Since these have already been identified as metallic using signal amplitudes from the first two layers, the lack of a signal on the backstop reliably identifies them as aluminum smaller than 0.4 mm.

4.4 Penetrator Size/Accuracy: Estimate from Acoustic Signals

The acoustic signal amplitude on the first layer can provide some indication of particle size. Presently, only a narrow range of particle sizes has been used in impact tests with the resistive grid. There is not yet adequate data on a wide range of particle sizes to generate a reliable amplitude-size relationship. However, there is a more extensive data set on the same thickness of Kapton films but without the resistive grid plating (from earlier hypervelocity shots at the University of Kent in Canterbury). This data indicates acoustic signal amplitude is independent of speed and particle density, and appears linearly proportional to particle diameter, or more precisely, to the circumference of the hole produced in the film. The incident angle plays a role in the circumference. Currently this type of relationship can provide only a rough estimate of size (with a range from half to double). It is most useful as a check on size determinations provided by the resistive grid instrument.

4.5 Penetrator Size Estimate from Grid Lines Cut

The determination of the penetrator size can be established statistically from the change in resistance of the resistive grid measurement, as determined from the number of lines of the grid that are cut. This determination is based on two functions. For simplicity only spherical particles are considered, while irregular particles would introduce a third function relating to the departure from sphericity. The first function is dependent on the point of impact of the penetrator in relation to the position of the grid lines. This relationship is defined by the geometry of the grid lines and the angle of incidence of the impacting penetrator relative to the grid line orientation. This function, for the simple geometry of a normal incident impact, is indicated in Fig. 12 as a probability of the number of grid lines cut in terms of the hole created in the grid by the penetrator.

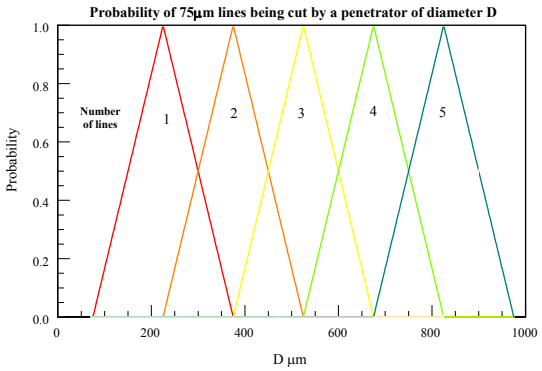

Figure 12. Probability of lines broken vs. object size

A test-based exemplar illustrates nominal grid behavior. Test E1's shot 15 (EIL log #2741) featured a launch package of three 0.2 mm SLG projectiles; one impacted the grid at 5.811 km/s at an angle of 33°. The impact broke one line of the test grid, resulting in a change in electrical resistance of 2.1 Ω, an outcome depicted in Fig. 13.

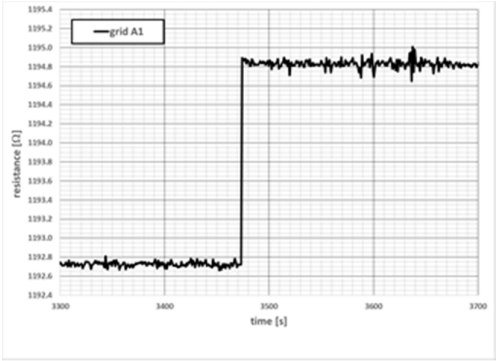

Figure 13. Grid resistance as a function of test elapsed time, demonstrating grid performance.

The line break probability relationship can be calculated for other than normal incident impacts and grid orientation; however, it should be understood that uncertainty in the determination of the impact angle and the orientation of the grid relative to the impact angle would contribute to uncertainty in the probability distribution.

The second function needed to determine the penetrator size requires a consistent relation between penetrator size, material, and velocity, in comparison to the size of the hole that is created by the impact. This relationship must be determined empirically and is limited by the physical test restrictions and the statistical variation of a less than infinite number of tests. In practice the tests used to determine this relationship for SDS were limited to less than 50 impacts of particles that ranged from 200 to 1000 µm diameter (specifically 200, 300, 400, 500 and 1000 µm). Most were with stainless steel (440C) and aluminum (2017-T4) spheres, with two tests using 200-micron aluminum oxide penetrators. The majority of the conducted tests were at about 7 km/s. The variation of the holes created by these tests in is illustrated in Fig. 14.

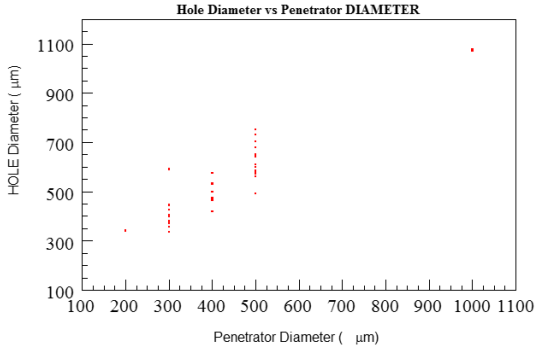

Figure 14. Hole Diameter vs Penetrator Diameter

The distribution of the hole diameter to penetrator diameter varies with penetrator size, and the ratios are given in Tab. 3 for the 300, 400, and 500 micron penetrators.

Table 3. Mean Hole Sizes

PENETRATOR SIZE (µm)	MEAN HOLE SIZE (µm)	STANDARD DEVIATION
300	412	64
400	492	50
500	622	69

These two distribution must be accounted for in determining the probability of a penetrator to a severed given number of lines. If we convolve the distribution of the ratio of penetrator to hole diameter with the probability of a line being cut, we can obtain a functional relationship giving the probability distribution for a penetrator of given size cutting a specific number of grid lines. This probability distribution is given in Fig. 15 for the case of three lines being cut. Similar probability distributions can be determined if a wider range penetrator diameters are tested.

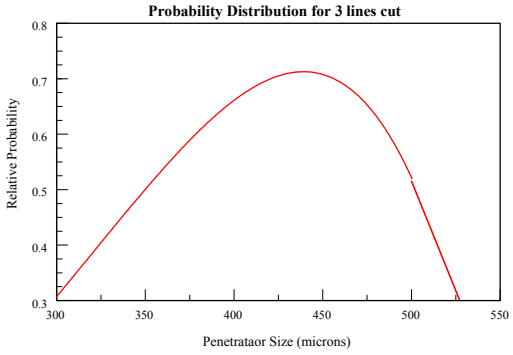

Figure 15. Probability Distribution for three lines cut

5 ANTICIPATED PERFORMANCE ON-ORBIT

Meteoroids may be distinguished from man-made orbital debris by relative velocity, directionality, and impact phenomenology. Fig. 16 depicts the predicted relative velocity distribution of micrometeroid (MM) and orbital debris (OD) at ISS altitude and is predicated upon the NASA ORDEM 3.0 (OD) and the Meteoroid Engineering Model (release 2) (MM) models.

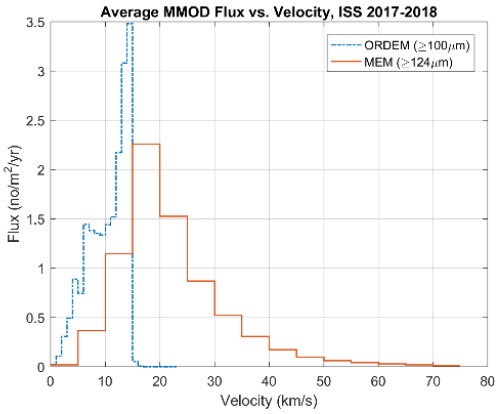

Figure 16. A comparison of MM and OD flux at ISS altitude over the nominal mission

The two environmental components exhibit distinct features in directionality that will be used to discriminate the components. Fig. 17 compares the flux directionality distributions.

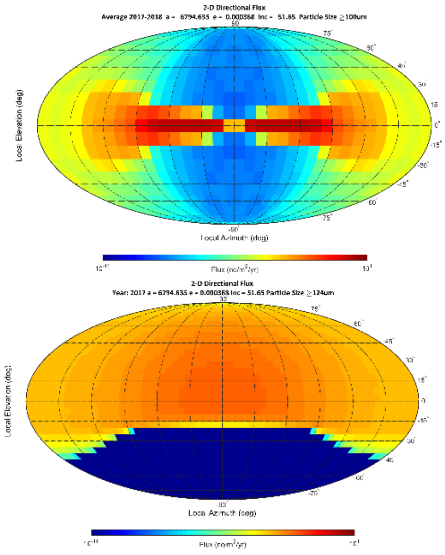

Figure 17. (Top) the distribution of OD flux in the local vertical-local horizontal plane, the ISS direction of motion being at the origin (Bottom) the corresponding MM flux distribution

Due to the difficulty and questionable extension of HVI and modeling results to MM velocities, some discrimination methodologies may require development during the on-orbit SDS initialization and checkout phases.

5.1 Non-Sensor Impacts and False Alarms

A common centering punch has been used in the laboratory to inject an acoustic signal of relatively constant magnitude and duration. These inputs are referred to as "taps." Taps on the sensor structure, including the bare sensor frame and support gussets, were observed during science testing to produce measurable acoustic signal on adjacent acoustic sensors. There is a high probability that the sensor's lateral or rear surface areas will be impacted. However, these areas are covered with thermal blankets and it is anticipated that these will tend to increase the threshold size for impactors reaching the structure and thereby lessen the probability of impact and observation. It is further anticipated that the localized nature of such impacts, likely registering only on the acoustic sensor nearest the impact point, will inform a rubric to remove these signals. Other sources of acoustic noise may include, but are not limited to, terminator passage, the ISS mechanical noise environment, and visiting vehicle's plume impingement or docking impulse. Grid-related phenomena may include broken or reconnected grid lines and electromagnetically induced noise due to illumination of the sensor by ground-based radars. Noise and false alarm mitigation may be accomplished through setting the sensor threshold, gain, or persistence (the number of pulses required to indicate a valid signal). Sensors also may be commanded off for decision making, though their signal is recorded.

5.2 Using the Results to Update ORDEM

To simulate how collected data will contribute to modeling the small particle environment, NASA's ORDEM 3.0 engineering model can be used to simulate an observing run of a given length of time with a discrete integer number of impacts, and proceed to fit the model flux. This can be repeated in a Monte Carlo manner to establish the uncertainties in this process.

Figure 18 shows where the debris flux is correctly described by ORDEM 3.0 and the instrument operates for the nominal 2 years. The colored curves estimate the uncertainty range (at 1-sigma, 90%, and 95% confidence limits) of the model fitting process. These curves show where the combination of number of impacts that occur and the number of lines severed for each impact determines how accurately the flux can be measured. Note that below about 60 μm, the instrument is incapable of making any meaningful measurements, as would be expected with the 75 μm wire spacing and wire width. A large region of uncertainty between about

70 and 200 µm corresponds to the inability to resolve sizes well when only one line is severed. For sizes above 200 µm, there are too few predicted impacts to provide meaningful statistics. While it is possible to establish upper limits for this case, not enough impacts can be guaranteed to be confident to firmly establish lower limits. Observations are needed for a longer time (or with more detectors representing a larger area) to improve these statistics. Fig. 19 shows the same information as Fig. 18, but for a 3-year observing time. In this case, there is some modest improvement in narrowing the upper and lower bounds of the uncertainties.

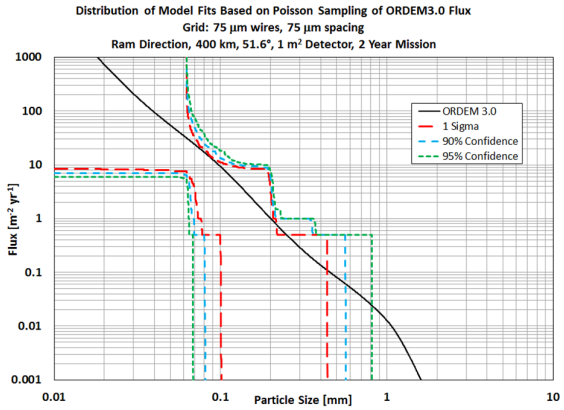

Figure 18. This chart represents a Monte Carlo simulation of impacts on the detector sampled using the ORDEM 3.0 model where, for each Monte Carlo run, the flux curve is fitted separately and statistics on the different Monte Carlo fits are accumulated.

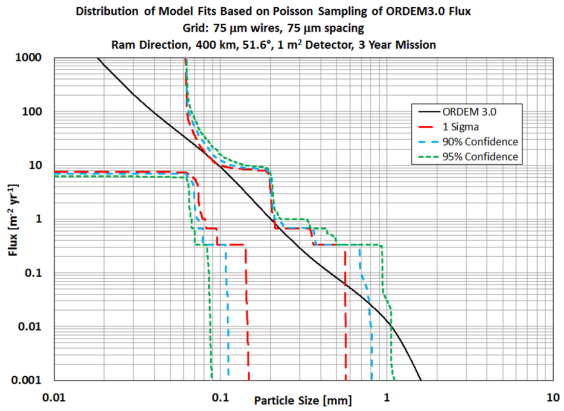

Figure 19. This chart is equivalent to Fig. 18, but for a 3-year observation time. This longer observation time shows some narrowing in the uncertainty range, but there is still limited information for sizes above about 200 µm.

Another way to analyze the instrument resolution is to assume that the environment is different from the model prediction by some amount. Then it can be determined how long the instrument would need to observe the environment before analysts could reject the hypothesis that the flux is the same as the model ORDEM 3.0 value. A 4-year observation time is insufficient to resolve unambiguously a factor of two uncertainty in the flux model. Modeling indicates that a flux ten times higher than the ORDEM 3.0 model flux can begin to be resolved, at least at sizes below about 200 µm after only 6 months of observations. However to resolve at sizes larger than 200 µm, observations would need to be extended past 1 year.

In summary, the current technology demonstration experiment will provide some insight into the particle flux from about 70 to 200 µm in size, even after the nominal 2-year mission, if the actual flux is up to a factor of ten times larger than the model flux. However, the exposure area, mission length, and wire resolution of the current instrument are insufficient to resolve if the actual flux is different from the model flux by only a factor of two or less. This resolution could be improved by integrating data from other instruments that would increase the total exposure area-time product, or by integrating data taken from different orbits – especially other altitudes. It is also possible that the size estimate from the acoustic sensors can be used to improve the resolution of the size estimate based upon severed grid lines only.

6 FOLLOW-ON SENSORS

The SDS experience will help improve detection and characterization technology. NASA ODPO is pursuing additional flight opportunities to deploy DRAGONS at higher altitudes. The primary target will be sun-synchronous orbits in the 700 to 1000 km altitude region.

7 CONCLUSIONS

Characterization of the small debris environment in LEO is an important and difficult task. *In-situ* sensors at ISS and higher altitudes are needed to accomplish that task. SDS will be used to determine the distribution of debris sizes, densities, and orbits. Fig. 20 shows the SDS systems engineer, Brian Dolan, standing next to the SDS after completion of ground testing.

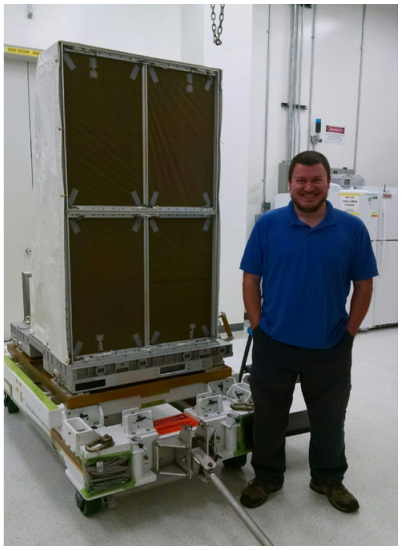

Figure 20. SDS ready for flight

The SDS soon will be tested at ISS. If successful, it will be a major step forward in monitoring the approximately 400 km-altitude environment and making it possible for future sensors to complete the characterization. That information will be used to update models critical to understanding the risks that the small debris environment poses to spaceflight in LEO.

8 REFERENCES

1. Liou, J.-C., Christiansen, E., Corsaro, R.D., Giovane, F., Tsou, P., and Stansbery, E. (2005). Modeling the Meteoroid Environment with Existing In Situ Measurements and with Potential Future Space Experiments. In *Proceedings of the 4th European Conference on Space Debris*, ESA SP-587, pp195-200.

2. Liou, J.-C., Burchell, M.J., Corsaro, R.D., Drolshagen, G., Giovane, G., Pisacane, V., and Stansbery, E. (2009). In situ measurement activities at the NASA Orbital Debris Program Office. In *Proceedings of the 5th European Conference on Space Debri*s, ESA SP-672.

3. Corsaro, R.D., Giovane, F., Liou,J.-C., Burchell, M.J., Cole, M.J., Williams, E.G., Lagakos, N., Sadilek, A., Anderson, C.R. (2016). *J. Acoust. Soc. Am.* **140**(2), pp1429-1438.